Carbonates and Evaporites (2022) 37:38
https://doi.org/10.1007/s13146-022-00785-2

ORIGINAL ARTICLE

The Kohlou barite deposit, Markazi Province, Iran: studies on rare earth element geochemistry, O and S isotopes, and fluid inclusions

Hedayat Hodaie Keveshk[1] · Farhad Ehya[1] · Ghodratollah Rostami Paydar[2] · Sara Maleki Kheymehsari[1]

Accepted: 4 May 2022 / Published online: 26 May 2022

Abstract

To determine the origin of the Kohlou barite deposit, comprehensive studies on petrography, rare earth element (REE) geochemistry, oxygen and sulfur isotopes, and fluid inclusions were performed. The Kohlou deposit is located 70 km northwest of Tafresh town in Markazi Province, Iran. Barite mineralization occurs as a stratabound manto at the contact of an overlying Eocene-aged volcano-sedimentary sequence with an underlying limestone horizon. Barite is accompanied by subordinate Fe- and Mn-oxides, calcite, and quartz. Field evidence including the presence of barite veinlets cross cutting host tuffs, and the brecciated host rocks cemented by barite suggest an epigenetic origin for the mineralization. The concentration of ∑REE is very low in barites, ranging from 0.22 to 16.41 ppm. Chondrite-normalized REE patterns show LREE enrichment relative to HREE, and mostly negative La and Ce anomalies. Gadolinium (Gd) anomalies vary from negative to positive in barite samples. The Ce/La and Y/Ho ratios, as well as La and Gd anomalies confirm a terrestrial source for barite from the Kohlou deposit. The $\delta^{18}O$ and $\delta^{34}S$ isotopic ratios in barites fall in narrow ranges of 1.7–2.7‰ and 14.6–16.3‰, respectively, implying that sulfate originated most likely from adjacent Miocene evaporites, with minor components of magmatic sulfur and oxygen carried in mineralizing fluids. Plots of $\delta^{34}S$ versus $\delta^{18}O$ do not show any similarity to barites from main modern marine and pedogenic settings, while overlap with the field represented by continental barite. Salinity values in fluid inclusions range from 8.28 to 23.25 wt% $NaCl + CaCl_2$ equivalent. Homogenization temperatures occupy the range of 139–272 °C. Fluid inclusion data indicate that basinal fluids, with minor contribution from meteoric water, were the source of mineralizing solutions. It is concluded here that faulting and brecciation of the host rocks provided the pathways needed for the upward migration of the basinal Ba-rich solutions. Barite precipitated where Ba-bearing fluids interacted evaporite deposits.

Keywords Rare earth element · Fluid inclusions · Sulfur isotopes · Oxygen isotopes · Barite · Kohlou

Introduction

Barite ($BaSO_4$) occurs in a considerably diverse range of sedimentary, igneous, and metamorphic rock types of all ages (Hanor 2000). It is found in soil, aerosol dust, and extra-terrestrial material (Brock-Hon et al. 2012; Griffith et al. 2018). In modern oceans, barite forms in various settings including hydrothermal vents, cold seeps, water columns, and sediments (Griffith and Paytan 2012; Crockford et al. 2019). On continents, barite precipitates in soils, sulfidic springs, and in the subsurface (Griffith et al. 2018). In all aforementioned settings, the fundamental requirement for the formation of barite is the interaction of two solutions, one containing Ba and the other sulfate, causing the environment to be supersaturated with respect to barite (Hanor 2000; Griffith et al. 2018). Hence, a key aspect in the study of barite deposits is to determine the sources of ore-forming elements and fluids.

Barite deposits are quite common in Iran, making it one of the most important barite producers in the world (McRae 2017). Barite mineralization occurred in Iran from Late Precambrian to Pliocene, but the most important periods of barite formation are Late Precambrian-Early Cambrian, Permian–Triassic, Cretaceous, and Paleogene (Ghorbani 2013). Apart from the Paleogene, barite

✉ Farhad Ehya
ehya.farhad@iau.ac.ir

[1] Department of Geology, Behbahan Branch, Islamic Azad University, Behbahan, Iran

[2] Department of Geology, Ahvaz Branch, Islamic Azad University, Ahvaz, Iran

mineralization occurs dominantly in dolomites and limestones. In contrast, Paleogene barite deposits are mainly associated with volcanic and volcanic-sedimentary rocks. Regarding the main sedimentary-structural zones of Iran, barite deposits are often found in Central Iran, Central Alborz, the Sanandaj-Sirjan Zone, and Urumieh-Dokhtar volcanic belt (Fig. 1; Ghorbani 2013).

Studies on some Iranian barite deposits show that they are of several types, including submarine hydrothermal (Ehya 2012; Ehya and Mazraei 2017; Alaminia and Sharifi 2018), Mississippi Valley Type (MVT) (Rajabzadeh 2007), terrestrial hydrothermal (Zarasvandi et al. 2014), sedimentary-exhalative (Derakhshi et al. 2019), and cold seeps (Hodaie Keveshk et al. 2021). Nevertheless, there is an incomplete picture of the range and types of barite deposits in Iran. Using field evidence, as well as REE geochemical, microthermometric, and isotopic data, we define the genesis of one of such understudied yet important barite deposits of Iran, the Kohlou deposit.

Geological setting

The Kohlou barite deposit (35° 00′ 15″ N, 49° 46′ 09″ E) is located 70 km northwest of Tafresh city, 1.5 km north of the Kohlou Pa'in village in Markazi Province, Iran, and is 2270 m above sea level. It is located in the Urumieh-Dokhtar Magmatic Arc (UDMA) (Fig. 1a). The UDMA forms a thick (> 4 km), linear assemblage of intrusive and extrusive igneous rocks extending along the entire Zagros orogenic belt. This complex is interpreted as an Andean type magmatic arc (Agard et al. 2011; Verdel et al. 2011). It consists of various rocks including diorite, granodiorite, gabbro, and granite, as well as basalt, trachybasalt, andesite, dacite,

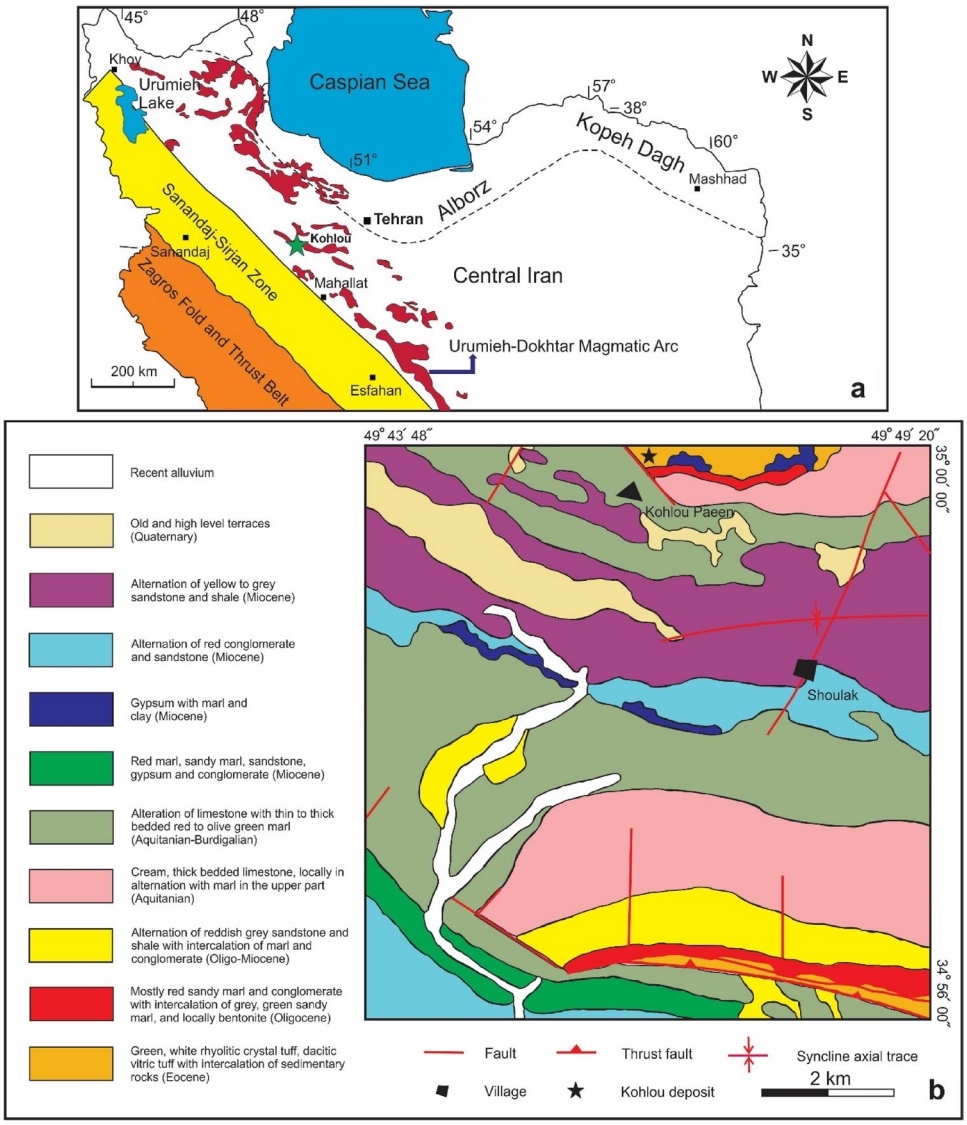

Fig. 1 **a** Location of the Kohlou barite deposit in the main tectonic zones of Iran (modified after Ghasemi and Talbot 2006); and **b** simplified geologic map of the Kohlou area (modified after Radfar and Kohansal, undated survey map)

trachyte, ignimbrite, and pyroclastic rocks (mainly tuff and agglomerate) (Alavi 1994). The oldest known intrusive body in the UDMA cross cuts the Upper Jurassic rock formations, while it is unconformably overlain by Lower Cretaceous fossiliferous limestones. The youngest deposits are Recent lava flows and pyroclastic rocks erupted from Quaternary volcanic craters. The Eocene is the age of peak magmatic activity, because large amounts of extrusive materials of this age interlayered with several horizons of nummulite-bearing limestones, are widespread across the UDMA. Petrochemical data indicate that the overall composition of igneous rocks in the UDMA is calc-alkaline (Mohajjel et al. 2003).

Figure 1b shows the geological map of the Kohlou deposit area. The region consists mainly of sedimentary rock units with ages from Eocene to Recent. A rock unit composed of green to white crystalline rhyolitic tuff, as well as dacitic glassy tuff with interlayers of Eocene calcareous sandstone and marl (it is hereinafter referred to as the volcano-sedimentary sequence), is the oldest rock unit cropping out in the deposit area. Barite mineralization occurs at the contact of the overlying volcano-sedimentary sequence with the lower strata, an unexposed horizon consisting of creamy to brown organodetritic sandy to marly nummulite-bearing limestone (Fig. 1b). Other rock units in the study area consist of Oligocene to Miocene sandy marl, marl, conglomerate, sandstone, shale, limestone and gypsum layers. Quaternary alluvial terraces and Recent alluviums are the youngest units in the study area.

Faults trending northwest-southeasterly, north-southerly, and northeast-southwesterly are the most important structural features in the study area (Fig. 1b). Close to the deposit, a reverse fault displaced beds of the volcano-sedimentary sequence at least 2 m (Fig. 2a). The western end of the Marq syncline is another structural feature in the region. Although not shown on the geological map of the deposit area (Fig. 1b), the orientation of the host rocks at the trench of the Kohlou deposit indicates that barite mineralization occurs along the hinge line of an asymmetric anticline whose southern limb dips more steeply than its northern one. The axis of this anticline trends east-westerly, plunging shallowly towards the west. Moreover, the contact between rock units in the southern limb of the anticline is mostly faulted, so that Eocene rock units serving as the host rock for barite mineralization is in contact with the younger rock units such as that composed of Miocene gypsum with marl and clay intercalations (dark blue in Fig. 1b). This indicates that faults in the southern limb of the anticline caused the older rock units to be thrusted over younger ones.

The Kohlou deposit is a small stratabound barite occurrence with a proved reserve of about 70,000 tonnes (Ganji 2015), exploited from a trench dug along the orebody; it is currently abandoned. Mining reports of the deposit are not available, so the initial dimensions of the orebody is unknown. However, field observations (including ore remains and excavated trenches for exploitation) indicate that mineralization occurred as a manto, 2–5 m wide. The trench that remained after exploitation has an approximate length, width and height of 70, 10 and 15 m, respectively.

Samples and methods

The macroscopic features of, and the relationships between, the ore and host rocks were investigated in the field. A total of 30 ore samples were selected along the strike of the barite orebody, with taking care to choose samples that are representative of the ore. Microscopic examinations were

Fig. 2 **a** Photograph showing a reverse fault in the Kohlou deposit that displaced layers of the volcano-sedimentary sequence; and **b** photograph from the Kohlou deposit trench showing barite manto at the contact between volcano-sedimentary rocks and limestone (looking west)

performed on 13 thin sections prepared from selected ore samples using a polarizing microscope.

Ten barite samples were analyzed for rare earth element (REE) and Y using the inductively coupled plasma-mass spectrometry (ICP-MS) method, by an Agilent 7900 model apparatus in the laboratory of the Iranian Mineral Processing Research Center (IMPRC) (Karaj, Iran). Only the most pristine barite specimens were selected for analysis; these were picked up by hand from crushed samples under a binocular microscope. Uncertainty of the measurements was achieved at the confidence interval of the 95% with a coverage factor of $k=2$, using an in-house standard. The detection limit is 0.01 ppm, except for La and Ce which are 0.05 and 0.1 ppm, respectively. Normalization of REE distributions in barite to chondrite (McDonough and Sun 1995) is a standard procedure, so it is followed here. Anomalies of La, Gd, Ce, and Pr were calculated using the equations proposed by Ehya (2012).

Three barite samples were analyzed for stable oxygen and sulfur isotopes in the Stable Isotope Research Laboratory at Arak University, Iran, using an Isoprime Isotope Ratio Mass Spectrometer (Elementar). Repetitive measurements were made on the samples and on in-house standards to verify the whole procedure. The accepted standard deviation (1σ) value for $\delta^{18}O$ is $\leq 0.3‰$, while that of $\delta^{34}S$ is 0.2‰, based on the reported specifications for the instrument. The isotopic ratios are presented in the δ notation as per mil (‰) relative to VSMOW for oxygen, and to VCDT for sulfur.

Four doubly polished wafers (~ 100 µm thick) were prepared from barite samples to study fluid inclusions, using a Zeiss microscope equipped with a Linkam THMS-600 heating-freezing stage at IMPRC. Standard compounds (cesium nitrate and n-hexane) were used to calibrate the apparatus, as its precision is ± 0.6 °C for heating and ± 0.2 °C for freezing measurements. Fluid inclusions were first subjected to heating and then freezing studies (Lawler and Crawford 1983). Salinity of aqueous H_2O–NaCl fluid inclusions was calculated from the ice melting temperatures ($T_{m,\ ice}$) using the equation of Bodnar (1993). Salinity of aqueous H_2O–NaCl–$CaCl_2$ fluid inclusions was calculated from ice ($T_{m,\ ice}$) and hydrohalite ($T_{m,\ hydro}$) melting temperatures using the model of Steele-MacInnis et al. (2011).

Results

Petrography and mineralogy

Host rocks

Barite mineralization at the Kohlou deposit occurs as a manto at the contact of a 300–350 m thick Eocene volcano-sedimentary sequence atop with a horizon of creamy to brown organodetritic sandy and marly nummulite-bearing limestone below (Fig. 2b). The volcano-sedimentary sequence consists either of green to white crystalline rhyolitic tuff, or dacitic glassy tuff with intercalations of calcareous sandstone and marl. Examination of calcareous sandstones reveals that they contain detrital particles 0.2–0.6 mm in diameter that are angular to semi-rounded, and show poor sorting and compaction. Detrital quartz, microcrystalline platy muscovite, and recrystallized quartz crystals, along with weak metamorphosed fragments and some fossils are contained in a carbonate groundmass impregnated with Fe-oxides and chlorite crystals (Radfar and Kohansal undated survey map).

The ore

Barite is often found as pure white to pink crystalline patches (Fig. 3a), making usually more than 95% of the ore. Impurities, especially in contact with the wall rocks, are mainly composed of host rock materials (Fig. 3b). Barite is sometimes found with Mn- and Fe-oxides. Manganese oxides often occur with dendritic aggregates on the surfaces of barite crystals. Iron oxides are commonly seen as rust and coatings on barite crystals (Fig. 3c). The fact that Mn- and Fe-oxides occur on barite crystals indicates that they formed in a late mineralization phase compared to barite. At the contact with wall rocks, there are barite veinlets a few centimeters thick, cross-cutting the host tuffs, showing clearly that mineralization is epigenetic (Fig. 3d). Further, brecciated host rocks, with spaces between clasts filled with barite (Fig. 3e) is consistent with syn- to post-faulting barite mineralization. It is very likely that faulting and brecciation of the host rocks provided the necessary pathways for migration of the mineralizing solutions, and thus played an important role for barite mineralization at Kohlou (see also below).

Petrographic studies indicate that the Kohlou's ore is very simple in terms of texture and mineralogy. Under microscope, barite is observed as large tabular crystals (up to 4 mm), as well as fine to coarse anhedral to subhedral crystals (up to 1 mm) (Fig. 4a). Calcite and, to a lesser extent, quartz are intergrown as fine to medium crystals with tabular barite crystals (Fig. 4b). Iron oxides are also formed as void-fillings, revealing their formation in a late mineralization stage.

The paragenetic sequence of the ore and host rocks in the Kohlou deposit is shown in Fig. 5. In the pre-mineralization stage, the volcano-sedimentary host rocks formed. The mineralization stage consists of two sub-stages, including early and late. The minerals barite, calcite, and a little quartz formed in the early sub-stage, followed by Mn- and Fe-oxides in the late sub-stage.

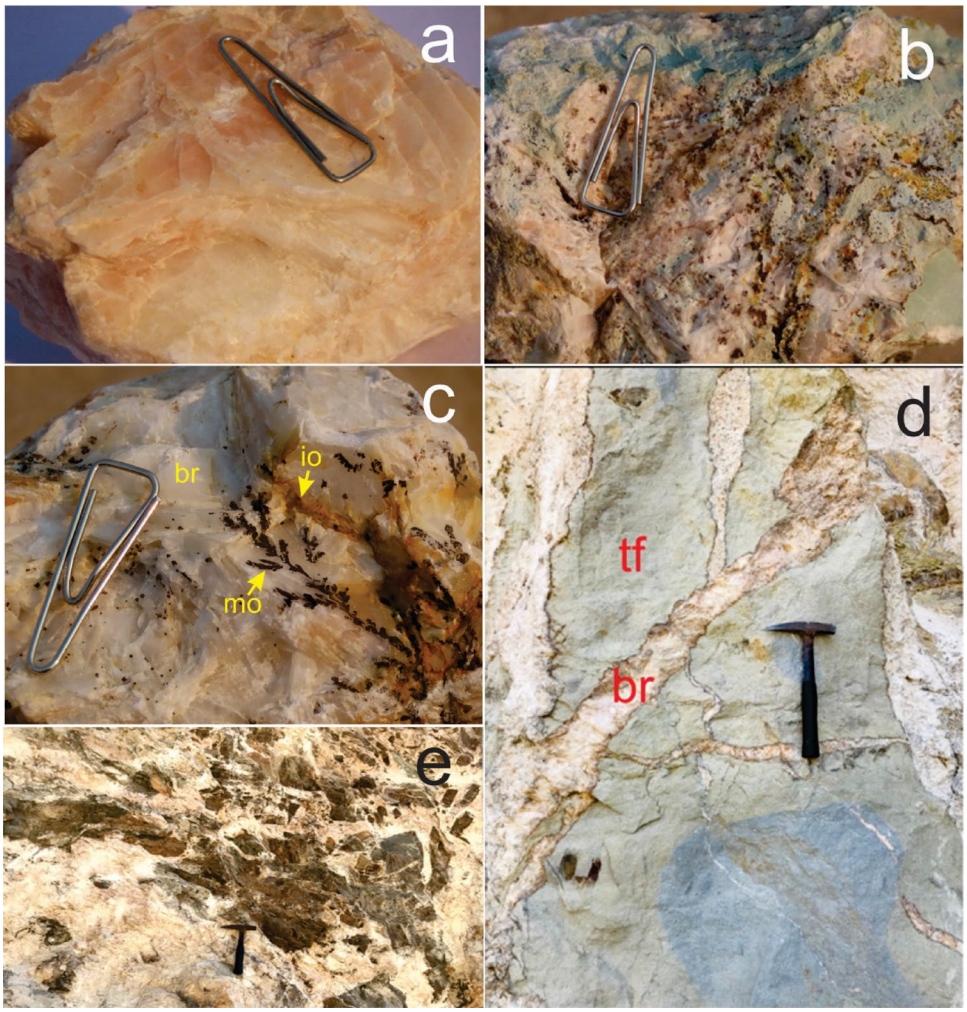

Fig. 3 **a** Photograph showing typical ore composed of white to pink barite; **b** photograph showing barite ore with impurities from host tuffs (pale green); **c** photograph showing barite ore (br) where Mn-oxides (mo) with dendritic aggregate are seen along with Fe-oxides (io); **d** photograph showing barite veinlets (br) cross-cutting the host tuffs (tf); and **e** photograph showing brecciation of host rocks, where the spaces between rock fragments (dark) are filled with barite (white)

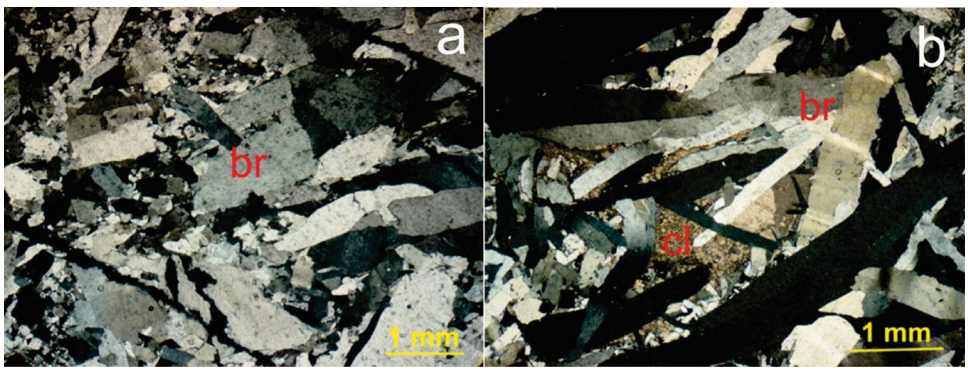

Fig. 4 **a** Photomicrograph showing large tabular barite crystals (br) intergrown with fine- to coarse-grained anhedral to subhedral crystals (cross polarized light); and **b** photomicrograph showing large tabular barite crystals (br). The spaces between barite crystals are filled, in some places, by anhedral to subhedral calcite crystals (cl) (cross polarized light)

REE geochemistry

The concentrations of rare earth element (REE) and Y in barite samples from the Kohlou deposit are provided in Table 1. The total concentration of REE (ΣREE) is low, between 0.22 and 16.41 ppm with an average value of 5.16 ppm. The total concentrations of light rare earth element (ΣLREE) and the total concentrations of heavy rare earth element (ΣHREE) are in the ranges of 0.15–16.32 and 0.07–0.82 ppm, respectively. The LREE/HREE ratios in barite samples range from 2.14 to 181.33, indicating that barite is enriched in LREE relative to HREE. The Y/Ho ratios range from 1.0 to 46.0. The Ce/La and Nd_{CN}/Yb_{CN} ratios vary from 1.0 to 4.4 and from 0.35 to 85.48, respectively. Barite samples show a negative La anomaly ($(La/La^*)_{CN} = -1.40–0.80$), except for one sample that does

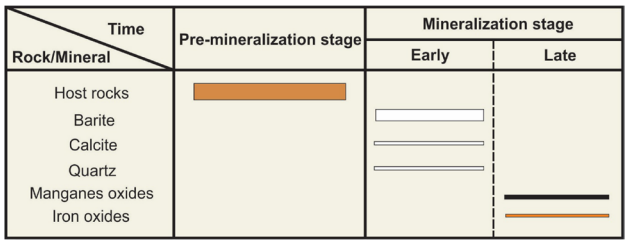

Fig. 5 Paragenetic sequence of the host rocks, ore and gangue minerals in the Kohlou deposit

not show an anomaly (1.00). The Gd anomalies vary from negative ($(Gd/Gd^*)_{CN}$ = 0.04–0.97) to weakly positive ($(Gd/Gd^*)_{CN}$ = 1.02–1.37), while a sample does not show an anomaly (1.00). In the case of Ce ($(Ce/Ce^*)_{SN}$), all samples show negative anomalies (0.00–27.57). Spectral interference of Eu with BaO during the ICP–MS analysis may occur, resulting in an analytical artifact (Greaves et al. 1989; Ehya 2012; Ehya and Mazraei 2017); hence, the interpretation of Eu concentration avoided herein. The chondrite-normalized REE patterns (McDonough and Sun 1995) for barite samples are shown in Fig. 6.

Oxygen and sulfur isotope systematics

The $\delta^{18}O$ and $\delta^{34}S$ values for three barite samples from the Kohlou deposit are given in Table 2 and shown in Fig. 7. The values of $\delta^{18}O$ are in a narrow range from 1.7 to 2.7‰. These values do not match with those of all Cenozoic seawaters, but are below the values specifying the Cenozoic seawater curve (Fig. 7; Turchyn and Schrag 2006). The $\delta^{34}S$ values also fall in a narrow range from 14.6 to 16.3‰. Like $\delta^{18}O$ values, the isotopic ratios of sulfur are not consistent with the values of Cenozoic seawaters, but instead are located below the Cenozoic seawater curve (Fig. 7; Paytan et al. 1998).

Fluid inclusion studies

Petrography of fluid inclusions

Based on the timing of fluid entrapment, two types of fluid inclusions were identified in barite samples from the Kohlou deposit, following the criteria provided by Roedder (1984) and Shepherd et al. (1985): primary and secondary. Secondary inclusions are found commonly in rows (Fig. 8a), while

Table 1 REE and Y contents of barite samples from the Kohlou deposit (all elements in ppm)

Sample	KL-1	KL-2	KL-3	KL-4	KL-5	KL-6	KL-7	KL-8	KL-9	KL-10
La	0.35	1.19	0.28	0.05	0.05	0.22	0.05	0.92	0.54	6.34
Ce	0.77	2.16	0.57	0.05	0.05	0.28	0.05	1.76	2.37	6.60
Pr	0.30	0.67	0.25	0.03	0.01	0.14	0.01	0.69	0.92	1.09
Nd	1.24	2.43	1.05	0.16	0.11	0.77	0.01	3.24	4.69	2.06
Sm	0.16	0.19	0.10	0.01	0.02	0.08	0.01	0.54	0.63	0.09
Eu	0.06	0.04	0.02	0.03	0.01	0.04	0.01	0.18	0.14	0.05
Gd	0.17	0.12	0.12	0.01	0.02	0.10	0.01	0.75	0.66	0.09
Tb	0.02	0.01	0.02	0.01	0.01	0.01	0.01	0.12	0.10	0.01
Dy	0.12	0.07	0.09	0.02	0.02	0.08	0.01	0.46	0.42	0.03
Ho	0.02	0.01	0.02	0.01	0.01	0.01	0.01	0.08	0.07	0.01
Er	0.03	0.02	0.03	0.01	0.01	0.01	0.01	0.11	0.13	0.01
Tm	0.01	0.01	0.01	0.01	0.01	0.01	0.01	0.01	0.01	0.01
Yb	0.01	0.01	0.02	0.01	0.01	0.01	0.01	0.03	0.07	0.01
Lu	0.01	0.01	0.01	0.01	0.01	0.01	0.01	0.01	0.01	0.01
Y	0.73	0.15	0.45	0.01	0.07	0.46	0.01	3.00	2.60	0.17
∑REE	3.27	6.94	2.59	0.42	0.35	1.77	0.22	8.90	10.76	16.41
∑LREE	3.05	6.80	2.39	0.34	0.27	1.63	0.15	8.08	9.95	16.32
∑HREE	0.22	0.14	0.20	0.08	0.08	0.14	0.07	0.82	0.81	0.09
LREE/HREE	13.86	48.57	11.95	4.25	3.38	11.64	2.14	9.85	12.28	181.33
Y/Ho	36.5	15.0	22.5	1.0	7.0	46.0	1.0	37.5	37.1	17.0
Ce/La	2.2	1.8	2.0	1.0	1.0	1.3	1.0	1.9	4.4	1.0
Nd_{CN}/Yb_{CN}	43.55	85.48	19.17	5.64	3.87	27.42	0.35	37.37	23.72	72.58
$(La/La^*)_{CN}$	0.35	0.46	0.34	0.80	-1.40	0.08	0.73	0.46	0.24	1.00
$(Gd/Gd^*)_{CN}$	1.16	0.97	1.02	0.24	0.04	1.37	0.24	0.53	1.00	1.16
$(Pr/Pr^*)_{SN}$	1.39	1.41	1.41	1.17	0.50	1.05	2.39	1.25	1.18	1.67
$(Ce/Ce^*)_{SN}$	0.44	0.50	0.40	0.27	0.51	0.32	0.51	0.44	0.49	0.57

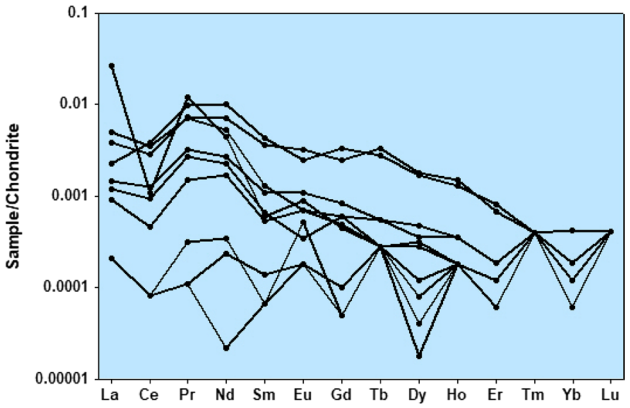

Fig. 6 Chondrite-normalized (McDonough and Sun 1995) REE patterns for barites from the Kohlou deposit

Table 2 Oxygen and sulfur isotopic compositions for barites from the Kohlou deposit

Sample	No. of repetitive runs	$\delta^{18}O_{VSMOW}$ (‰) ± 1σ	$\delta^{34}S_{VCDT}$ (‰) ± 1σ
KO1	3	+2.7 ± 0.3	+14.6 ± 0.2
KO2	3	+1.7 ± 0.3	+16.3 ± 0.2
KO3	3	+1.8 ± 0.3	+15.0 ± 0.2

primary inclusions are observed to be isolated and randomly distributed. Since secondary fluid inclusions show the post-formation history of barite, all measurements were made on primary fluid inclusions.

According to the type of phases present at room temperature and the homogenization behavior, two types of aqueous fluid inclusions are identified in the barite samples; liquid-rich biphase (L + V) inclusions homogenizing to the liquid phase, and monophase liquid (L) inclusions. The biphase inclusions are characterized by an aqueous liquid and a small vapour bubble that occupies 20–30 vol% of the inclusion. The size of these inclusions is in the range from 4 to 22 µm. They are observed in irregular shapes and, sometimes, negative crystals (Fig. 8b). The monophase inclusions are characterized by having only one aqueous liquid phase. The size of these inclusions is in the range from 5 to 20 µm. They have irregular and oval shapes (Fig. 8c).

Microthermometric results

Microthermometric measurements were performed on biphase fluid inclusions. A total of 63 inclusions were measured. The results of microthermometric studies and abbreviations used in the text are given in Table 3. To ensure that the fluid inclusions are completely frozen, they were cooled to − 100 to − 110 °C in freezing studies. During heating

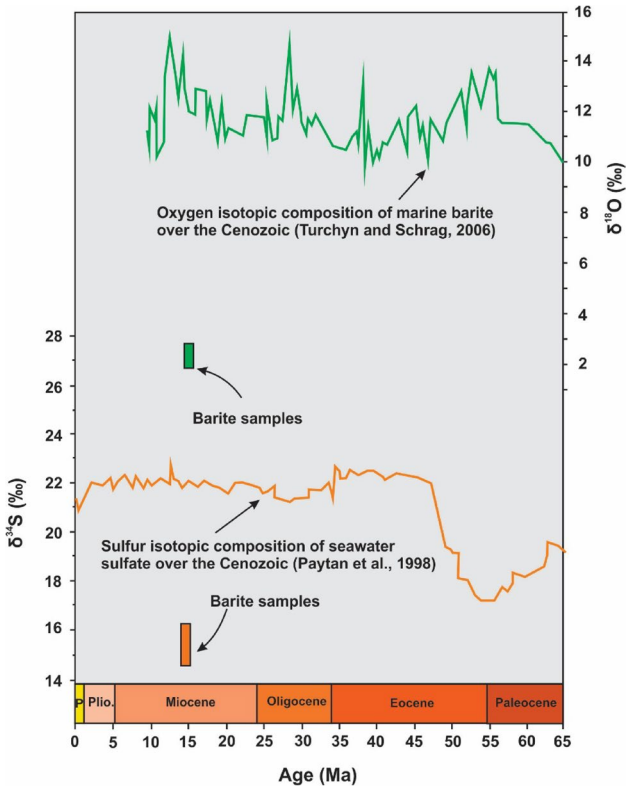

Fig. 7 The $\delta^{18}O$ and $\delta^{34}S$ values of barite from the Kohlou deposit compared with oxygen isotopic composition of marine barite (Turchyn and Schrag 2006) and sulfur isotopic composition of Cenozoic seawater sulfate (Paytan et al. 1998)

measurements, all inclusions were homogenized to the liquid phase.

The temperatures of the first ice melting (T_e) in some fluid inclusions is − 52 °C, indicating the presence of H_2O–NaCl–$CaCl_2$ brine system in the inclusions (Roedder 1984; Shepherd et al. 1985; Steele-MacInnis et al. 2011). In some inclusions, however, T_e values is between − 42 and − 45 °C. These inclusions are considered to represent H_2O–NaCl brine system. The observed deviation from the stable eutectic temperature (− 21.1 °C) for the H_2O–NaCl system may reveal the presence of divalent cations, probably Ca^{2+}, within the fluid (Roedder 1984; Shepherd et al. 1985; Goldstein and Reynolds 1994). In the H_2O–NaCl–$CaCl_2$ fluid inclusions, hydrohalite was formed while the liquid phase froze. In these inclusions, ice was the last phase to melt. The temperatures of the last ice ($T_{m,\ ice}$) and hydrohalite ($T_{m,\ hydro}$) melting are in the ranges from − 24.0 to − 11.1 °C, and from − 37.4 to − 23.2 °C, respectively. Salinities calculated based on the $T_{m,\ ice}$ and $T_{m,\ hydro}$ fall in the ranges from 2.29 to 14.66 wt% NaCl equivalent, from 4.29 to 16.19 wt% $CaCl_2$ equivalent, and from 15.03 to 23.25 wt% NaCl + $CaCl_2$ equivalent. The $T_{m,\ ice}$ in H_2O–NaCl fluid inclusions varies from − 17 to − 5.3 °C, corresponding to

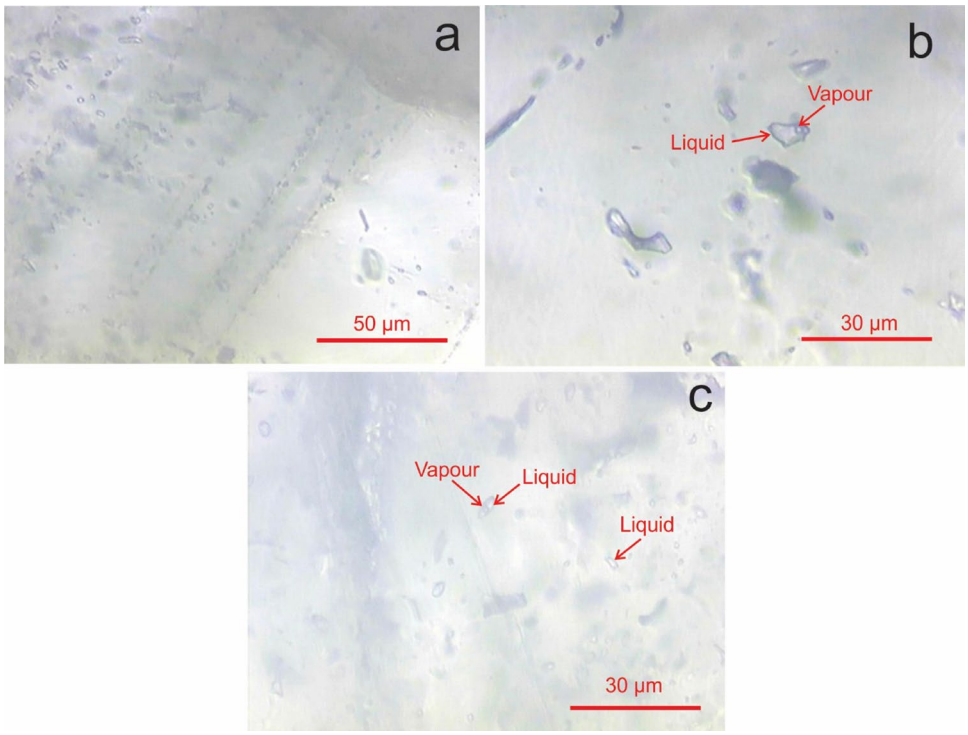

Fig. 8 Types of fluid inclusions recognized based on the criteria provided by Roedder (1984) and Shepherd et al. (1985) in barite crystals; **a** Secondary fluid inclusions; **b** primary aqueous liquid-rich biphase (L + V) inclusions; and **c** primary aqueous monophase liquid (L) inclusions

Table 3 Summary of microthermometric results for fluid inclusions in barite from the Kohlou deposit

Inclusion system	$T_{m,hydro}$ (°C)	T_e (°C)	$T_{m,ice}$ (°C)	T_h (°C)	Salinity (wt% NaCl eq.)	Salinity (wt% $CaCl_2$ eq.)	Salinity (wt% NaCl + $CaCl_2$ eq.)	*N*
H_2O–NaCl–$CaCl_2$	− 37.4/− 23.2	− 52	− 24/− 11.1	139/272	2.29/14.66	4.29/16.19	15.03/23.25	7
H_2O–NaCl	–	− 42/− 45	− 17/− 5.3	162/255	8.28/20.22	–	8.28/20.22	56

T_e first ice melting temperature, $T_{m,ice}$ last ice melting temperature, $T_{m,hydro}$ last hydrohalite melting temperature, T_h homogenization temperature to liquid, *N* number of measurements

salinities from 8.28 to 20.22 wt% NaCl equivalent. Homogenization temperatures (T_h) vary from 139 to 272 °C.

Discussion

REE patterns

The chondrite-normalized REE patterns (McDonough and Sun 1995; Fig. 6) indicate that LREE are enriched in barite relative to HREE. The LREE/HREE (2.14–181.33) and Nd_{CN}/Yb_{CN} (3.87–85.48, except for one sample (0.35)) ratios are consistent with this. The LREE enrichment is a common feature in barite because the similarity of the LREE ionic radius (compared to HREE) to Ba^{2+} causes LREE to be concentrated when REE is substituting in the barite lattice (Guichard et al. 1979; Wu et al. 2021).

The Ce/La ratio in deep-sea barites is < 1 and similar to that of seawater, while in terrestrial (vein) barites it is > 1 and similar to that of basic rocks and clays (Guichard et al. 1979). The Ce/La ratio in barites from the Kohlou deposit varies from 1.0 to 4.4 with an average value of 1.76 (Table 1), similar to that in terrestrial barites. Marine chemical sediments are commonly characterized by $(La/La^*)_{CN}$ and $(Gd/Gd^*)_{CN}$ ratios above unity, irrespective of age (Alexander et al. 2008). In contrast, Kohlou barite shows $(La/La^*)_{CN}$ ratios < 1 ($(La/La^*)_{CN}$ = -1.0–0.80) (except for one sample where it is 1), and $(Gd/Gd^*)_{CN}$ ratios from < 1 ($(Gd/Gd^*)_{CN}$ = 0.04–0.97) to slightly > 1 ($(Gd/Gd^*)_{CN}$ = 1.00–1.37). Therefore, Ce/La ratios and La and Gd anomalies are inconsistent with a marine origin for barite from the Kohlou deposit, instead indicating a terrestrial source.

The Y/Ho ratios in barite samples from the Kohlou deposit show values from 1.0 to 46.0, with an average value of 22. This mean value is close to its chondritic ratio (Y/Ho = 28; McDonough and Sun 1995), while it is considerably less than its value in seawater (Y/Ho = 101;

Bao et al. 2008). Therefore, the Y/Ho ratios do not confirm a marine provenance for the studied barite samples, but implying again a terrestrial origin.

As provided in Table 1 and shown in Fig. 9, the $(Ce/Ce^*)_{SN}$ ratios indicate that all, but one, barite samples have negative Ce anomalies. Open seawater and related deposits exhibit such anomalies, because Ce is oxidized to insoluble Ce^{4+} in seawater and is removed rapidly (Pattan et al. 2005). Since REE geochemical indicators rule out marine origin for barite, the similarity of Ce anomalies in barite samples with those of seawater and marine sediments indicates that mineralizing solutions sourced possibly from seawater. Basinal brines originating from trapped seawater in the pores of sedimentary rocks were involved in the formation of many base-metal and barite-celestite deposits (Kharaka and Hanor 2003; Abidi et al. 2012; González-Sánchez et al. 2017; Saintilan et al. 2019). These waters interact effectively with the rocks trapped in them, so their chemical composition can be significantly different from the initial composition of seawater. The drift of Y/Ho ratio in barite samples from that in seawater could be caused by such interactions. It is noted that the fact that mineralizing solutions originated likely from seawater does not mean that barite is marine in origin, because basinal fluids can precipitate barite epigenetically (terrestrial barite) where suitable conditions are met. The role of basinal waters as mineralizing solutions in barite formation at the Kohlou deposit is further confirmed by fluid inclusion studies (see below for more explanation).

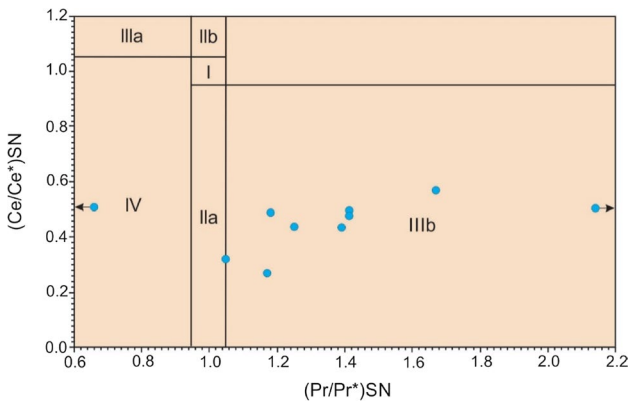

Fig. 9 $(Ce/Ce^*)_{SN}$ versus $(Pr/Pr^*)_{SN}$ diagram for barites from Kohlou deposit (after Bau and Dulski, 1996; Shields et al. 2004). Field I: no anomaly; field IIa: positive La anomaly causes an apparent negative Ce anomaly; field IIb: a negative La anomaly produces an apparent positive Ce anomaly; field IIIa: real positive Ce anomaly; field IIIb: real negative Ce anomaly; field IV: positive La anomaly disguises a positive Ce anomaly

Oxygen and sulfur isotope geochemistry

The Kohlou's barite has uniform isotopic compositions: $14.6‰ \leq \delta^{34}S \leq 16.3‰$ and $1.7‰ \leq \delta^{18}O \leq 2.7‰$. The fact that isotopic composition of sulfur in barite samples is large positive indicates that the source of sulfur is seawater sulfate. The gypsum beds contained in nearby Miocene marine sediments could be an easily accessible source of marine sulfate for barite mineralization at the Kohlou deposit (Fig. 1b). However, sulfate of the barite samples is slightly richer in ^{32}S than the sulfate of the Miocene seawater (Fig. 7). Because of the presence of volcanic igneous rocks in host rocks to the barite mineralization in Kohlou deposit, the lower values of $\delta^{34}S$ in barite samples compared to those of Miocene seawater can be due to the contamination of mineralizing fluids by volcanic rocks ($\delta^{34}S$ from -3 to $+1‰$; Hoefs 2009).

The $\delta^{18}O$ values in barite samples are also much lower than those in the Miocene seawater (Fig. 7). Although the $\delta^{18}O$ values in igneous rocks is in the range of 5.5–7.0‰ (Taylor 1968), much lower values from -1.2 to 4.8 ‰ have also been reported in volcanic rocks with rhyolite to dacite compositions (Boroughs et al. 2012). Similar to the isotopic composition of sulfur, it is possible that impregnating of the ore-forming solutions with a magmatic component reduced the $\delta^{18}O$ values in the studied barite samples. Therefore, oxygen and sulfur isotopic data demonstrate that sulfate in barite from the Kohlou deposit originated most likely from closely located Miocene evaporites, with some contamination from host rocks.

Plots of $\delta^{34}S$ versus $\delta^{18}O$ values of barite are used to discriminate between barite of contrasting origins (e.g., Johnson et al. 2004, 2009; Griffith et al. 2018). Figure 10 compares isotopic compositions of the Kohlou deposit to those of Miocene seawater (Turchyn and Schrag 2006; Paytan et al. 1998) and modern barite-producing geological environments (Griffith et al. 2018 and references therein). The Kohlou deposit differs with pelagic barites with regards to both $\delta^{34}S$ and $\delta^{18}O$ values. The $\delta^{34}S$ values in Kohlou barites are lower than that of Miocene seawater, while in pelagic barites they are close to that of present-day seawater. Marine pelagic barites display $\delta^{18}O$ values slightly lower than that of seawater sulfate (Griffith et al. 2018), whereas $\delta^{18}O$ values in the Kohlou barites are significantly lower than those of Miocene seawater. Marine hydrothermal barite has $\delta^{18}O$ and $\delta^{34}S$ values ranging from similar to, to slightly lower, to considerably higher than those of modern seawater (Fig. 10; Ehya 2012; Griffith et al. 2018). In contrast, Kohlou barites have $\delta^{34}S$ and $\delta^{18}O$ values that are much less than expected for Miocene seawater. Thus, pelagic and marine hydrothermal barites are not analogs for barite from the Kohlou deposit.

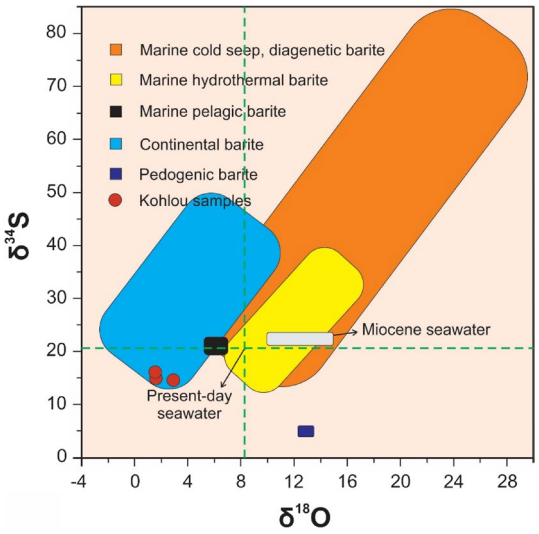

Fig. 10 Plot of $\delta^{34}S$ versus $\delta^{18}O$ values of barite from the Kohlou deposit compared to isotopic composition of Miocene seawater (Turchyn and Schrag 2006; Paytan et al. 1998) and to barites from main modern settings in which barite is formed (data from Griffith et al. 2018 and references therein)

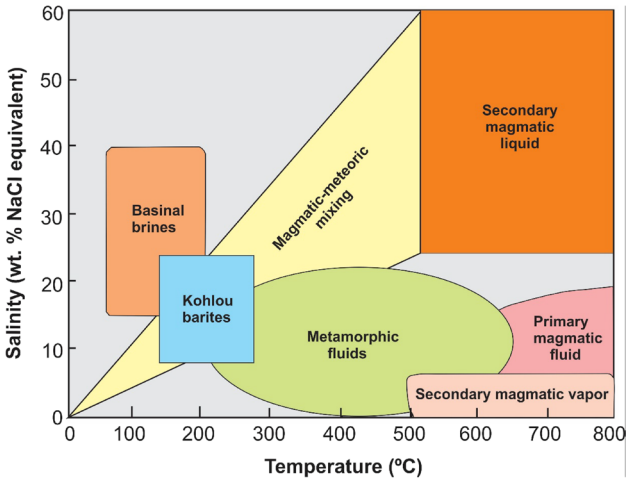

Fig. 11 T_h-salinity plot for aqueous fluid inclusions in barite from the Kohlou deposit (Bodnar 1999)

Although marine cold seep and diagenetic barites are often characterized by wide ranges of $\delta^{18}O$ and $\delta^{34}S$ values, from seawater-like values to values several times greater than those of present-day seawater (Griffith et al. 2018), few diagenetic barites with $\delta^{18}O$ values lower than that of seawater, and cold seep barite with little variability in $\delta^{18}O$ and $\delta^{34}S$ values are reported by Paytan et al. (2002) and Stevens et al. (2015), respectively. Considering that Kohlou barite has $\delta^{34}S$ and $\delta^{18}O$ values considerably lower than those of Miocene seawater, and that they show narrow ranges, lead to conclusion that diagenetic and marine cold seep barites also cannot be regarded as analogs for barites from the Kohlou deposit.

The $\delta^{34}S$ values in pedogenic barite samples from Lufkin Series in south-central Texas, USA, are the lowest values in barite formed today or in the recent past. However, they show higher $\delta^{18}O$ values than those of their sulfur sources (Griffith et al. 2018). Pedogenic barite is deposited commonly in humid, clay-rich soils under acidic conditions, and rarely in soils and paleosols of arid climates (Brock-Hon et al. 2012), with no economic importance. In addition to differences in $\delta^{34}S$ and $\delta^{18}O$ values between pedogenic and Kohlou barites (Fig. 10), the formation setting of pedogenic barite differs essentially with that of the Kohlou deposit and is thus a highly unlikely analog.

Continental barites (i.e., barites in sediments and crusts around the continental sulfidic springs) have $\delta^{34}S$ values ranging from slightly to considerably higher than that of the sulfide emanating from the spring. The source of oxygen in the continental sulfidic spring settings is poorly understood (Griffith et al. 2018). Unlike typical continental barite, the $\delta^{34}S$ values from Kohlou deposit are less than those in their probable source of sulfur (Miocene evaporites), as the reason was discussed above. However, the fact that data points fall in the continental barite field (Fig. 10) indicate that barite from the Kohlou deposit is from a continental origin. This interpretation is in line with Ce/La ratio, and La and Gd anomalies in barites.

Source of ore-forming fluids

Barite from the Kohlou deposit precipitated from relatively low- to high-salinity (8.28–23.25 wt% $NaCl + CaCl_2$ equivalent) fluids, as deduced from microthermometric studies. High-salinities of the fluids is well compatible with salinity of the basinal brines, while low-salinities indicate most likely the brine dilution by meteoric water (González-Sánchez et al. 2017) (Fig. 11). The lower extreme of the homogenization temperature range (139–272 °C) for barite-hosted fluid inclusions is consistent with the basinal water temperatures, while the upper limit exceeds the temperature range of the basinal brines in Fig. 11. However, basinal fluids with temperatures > 300 °C are reported in some sedimentary basins, for which high-temperatures is attributed to derivation from a great depth (Gleeson et al. 2003; Kyser 2007). Therefore, it can be concluded that mineralizing brines sourced from basinal solutions with a likely minor contribution from meteoric waters.

Mode of ore formation

Field studies provide evidence clearly indicating an epigenetic origin for barite mineralization at Kohlou. This evidence includes the presence of host tuffs cross cut by

barite veinlets at the ore-wall rock interface, as well as the brecciated host rocks cemented by barite (Figs. 3d and e). Epigenetic barite precipitates within a previously deposited host sediment by reaction between Ba-rich fluids and marine evaporites and/or buried evaporative marine waters (Hanor 2000; Forjanes et al. 2020). Based on fluid inclusion data, Ba-enriched basinal fluids, with minor contribution from meteoric water, supplied the mineralizing solutions to the Kohlou barite deposit. Moreover, sulfur isotopes suggest that nearby Miocene evaporites (gypsum) provided the needed sulfate for barite mineralization. The Eocene host rocks came into contact with Miocene evaporite-bearing strata by thrust faulting (Fig. 1b). Overall, it is very likely that faulting and brecciation of the host rocks provided the conduits required for the upward migration of the basinal Ba-rich solutions. Barite precipitated as a manto at the contact of the overlying volcano-sedimentary sequence with the underlying limestone horizon, where Ba-bearing fluids encountered gypsum beds. According to Forjanes et al. (2020), interaction between Ba-bearing aqueous solutions and gypsum leads to the development of dissolution–precipitation reactions, resulting in the replacement of gypsum by barite. This mode of ore formation is also stated, for example, by González-Sánchez et al. (2017) for barite deposits at Múzquiz, Coahuila in northeastern Mexico.

The barite deposits at Múzquiz consist of mantos (up to 20 km long and 1–5 m in thickness) with an epigenetic and stratabound character, emplaced in limestone at the contact of two Lower Cretaceous limestone formations. The ore in the Múzquiz is composed of nearly pure barite, with the gangue minerals including calcite, minor celestine, amorphous silica, Fe-(oxy) hydroxides, and Mn-oxides (González-Sánchez et al. 2017). The brecciated limestone cemented by barite is commonly found. The Múzquiz barite shows sedimentary or diagenetic features such as banded rhythmites and "chicken-wire" structures pseudomorphically replaced by barite, and the presence of organic material. González-Sánchez et al. (2017) suggested that barite deposits at Múzquiz were formed through the replacement of pre-existing anhydrite horizons in the host limestone formation, by mineralizing fluids that was dominantly basinal brines.

Comparing Kohlou with Múzquiz indicates both similarities and differences between these two deposits. Similarities include the pureness of barite, ore mineralogy (excluding celestine in Kohlou deposit), host rocks (excluding pyroclastic rocks in Kohlou deposit), presence of barite-cemented brecciated host rocks, similar $\delta^{34}S$ values (mean 16.9‰ for Múzquiz deposits), fluid inclusion salinities (7.9–27 wt% NaCl equivalent in Múzquiz deposits), and brine system (being dominated by $CaCl_2$). The differences are the lack of replacement structures and organic matter in Kohlou, as well as lower temperatures (59–155 °C) for ore-forming fluids at Múzquiz compared to those of the Kohlou (139–272 °C). The later probably reflects the fact that mineralizing solutions in Kohlou derived from a greater depth than in Múzquiz. The absence of replacement textures in the Kahloo deposit, despite all the evidence indicating the formation of barite via the exposure of Ba-rich brines to evaporitic beds, may be due to the fact that these textures are probably disappeared by post-deposition processes (e.g., recrystallization effects). Regardless of these similar and contrasting features, the mechanism of barite formation in these two deposits (encounter of Ba-rich brines with evaporites) seems to be the same based on the available evidence.

Conclusions

The Kohlou barite deposit consists of high-grade barite with a stratabound and epigenetic signature, emplaced as a manto at the contact of an Eocene volcano-sedimentary sequence with a limestone horizon. The REE-Y elemental ratios reveal a terrestrial source for barite from the Kohlou deposit, instead of a marine genesis. Results of stable S and O isotope analyses in barite states that sulfur and oxygen sourced from nearby Miocene evaporites with little contamination from magmatic components. Microthermometric studies on fluid inclusions showed a $CaCl_2$-rich brine system in fluids, and that mineralizing brines largely derived from basinal solutions with minor contribution from meteoric waters. Field evidence, as well as REE geochemical, microthermometric, and isotopic data demonstrate that the Kohlou barite deposit is generated through the encounter of basinal Ba-rich solutions with evaporites.

Acknowledgements This research was conducted as partial fulfillment of the requirements for a Ph.D. degree in Economic Geology for the first author from the Behbahan Branch, Islamic Azad University. Funding this research was partly provided by the Iranian Mines and Mining Industries Development and Renovation (IMIDRO) Company, which is kindly acknowledged.

References

Abidi R, Slim-Shimi N, Marignac C, Hatira N, Gasquet D, Renac C, Soumarin A, Gleeson S (2012) The origin of sulfate mineralization and the nature of the $BaSO_4$–$SrSO_4$ solid-solution series in the Ain Allega and El Aguiba ore deposits, Northern Tunisia. Ore Geol Rev 48:165–179

Agard P, Omrani J, Jolivet L, Whitechurch H, Vrielynck B, Spakman W, Monie P, Meyer B, Wortel R (2011) Zagros orogeny: a subduction-dominated process. Geol Mag 148:692–725

Alaminia Z, Sharifi M (2018) Geological, geochemical and fluid inclusion studies on the evolution of barite mineralization in the Badroud area of Iran. Ore Geol Rev 92:613–626

Alavi M (1994) Tectonics of the Zagros Orogenic Belt of Iran: new data and interpretations. Tectonophysics 229:211–238

Alexander BW, Bau M, Andersson P, Dulski P (2008) Continentally derived solutes in shallow Archean seawater: rare earth element

and Nd isotope evidence in iron formation from the 2.9 Ga Pongola Supergroup, South Africa. Geochim Cosmochim Acta 72:378–394

Bao SX, Zhou HY, Peng XT, Ji FW, Yao HQ (2008) Geochemistry of REE and yttrium in hydrothermal fluids from the Endeavour segment, Juan de Fuca Ridge. Geochem J 42:359–370

Bau M, Dulski P (1996) Distribution of yttrium and rare earth elements in the Penge and Kuruman iron-formations, Transvaal Supergroup, South Africa. Precambr Res 79:37–55

Bodnar RJ (1993) Revised equation and table for determining the freezing point depression of H_2O–NaCl solution. Geochim Cosmochim Acta 57:683–684

Bodnar RJ (1999) Hydrothermal solutions. In: Marshall CP, Fairbridge RW (eds) Encyclopedia of geochemistry. Kluwer Academic Publishers, Lancaster, pp 333–337

Boroughs S, Wolff JA, Ellis BS, Bonnichsen B, Larson PB (2012) Evaluation of models for the origin of Miocene low-$\delta^{18}O$ rhyolites of the Yellowstone/Columbia River Large Igneous Province. Earth Planet Sci Lett 313–314:45–55

Brock-Hon AL, Robins CR, Buck BJ (2012) Micromorphological investigation of pedogenic barite in Mormon Mesa petrocalcic horizons, Nevada USA: implication for genesis. Geoderma 179–180:1–8

Crockford PW, Wing BA, Paytan A, Hodgskiss MSW, Mayfield KK, Hayles JA, Middleton JE, Ahm ASC, Johnston DT, Caxito F, Uhlein G, Halverson GP, Eickmann B, Torres M, Horner TJ (2019) Barium-isotopic constraints on the origin of post-Marinoan barites. Earth Planet Sci Lett 519:234–244

Derakhshi MG, Hosseinzadeh MR, Moayyed M, Maghfouri S (2019) Metallogenesis of Precambrian SEDEX-type barite–(Pb–Cu–Zn) deposits in the Mishu mountain, NW Iran: constrains on the geochemistry and tectonic evolution of mineralization. Ore Geol Rev 107:310–335

Ehya F (2012) Rare earth element and stable isotope (O, S) geochemistry of barite from the Bijgan deposit, Markazi Province, Iran. Mineral Petrol 104:81–93

Ehya F, Mazraei SM (2017) Hydrothermal barite mineralization at Chenarvardeh deposit, Markazi Province, Iran: evidences from REE geochemistry and fluid inclusions. Afr Earth Sci 134:299–307

Forjanes P, Astilleros JM, Fernández-Díaz L (2020) The formation of barite and celestite through the replacement of gypsum. Minerals 10:189

Ganji A (2015) Barite mineralization in Iran. VI. BALKANMINE, Petrosani 2015

Ghasemi A, Talbot CJ (2006) A new tectonic scenario for the Sanandaj–Sirjan Zone, Iran. J Asian Earth Sci 26:683–693

Ghorbani M (2013) The economic geology of Iran, mineral deposits and natural resources. Springer Geology, Dordrecht. https://doi.org/10.1007/978-94-007-5625-0

Gleeson SA, Yardley BWD, Munz IA, Boyce AJ (2003) Infiltration of basinal fluids into high-grade basement, South Norway: sources and behaviour of waters and brines. Geofluids 3:33–48

Goldstein RH, Reynolds TJ (1994) Systematics of fluid inclusions in diagenetic minerals. SEPM short course notes, vol 31. SEPM Society for Sedimentary Geology, pp 199

González-Sánchez F, González-Partida E, Canet C, Atudorei V, Alfonso P, Morales-Puente P, Cienfuegos-Alvarado E, González-Ruiz L (2017) Geological setting and genesis of stratabound barite deposits at Múzquiz, Coahuila in northeastern Mexico. Ore Geol Rev 81:1184–1192

Greaves MJ, Elderfield H, Klinkhammer GP (1989) Determination of the rare earth elements in natural water by isotope-dilution mass spectrometry. Anal Chim Acta 218:265–280

Griffith EM, Paytan A (2012) Barite in the ocean-occurrence, geochemistry and palaeoceanographic applications. Sedimentology 59:1817–1835

Griffith EM, Paytan A, Wortmann UG, Eisenhauer A, Scher HD (2018) Combining metal and nonmetal isotopic measurements in barite to identify mode of formation. Chem Geol 500:148–158

Guichard F, Church TM, Treuil M, Jaffrezic H (1979) Rare earths in barites: distribution and effects on aqueous partitioning. Geochim Cosmochim Acta 49:983–997

Hanor JS (2000) Barite-celestite geochemistry and environments of formation. Rev Mineral Geochem 40:193–263

Hodaie Keveshk H, Ehya F, Rostami Paydar G, Maleki Kheymehsari S (2021) Rare earth elements geochemistry, O and S isotopic compositions, and microthermometric data of barite from the Kuh-Ghalagheh deposit, Markazi Province, Iran. Appl Geochem 135:105128

Hoefs J (2009) Stable isotope geochemistry, 6th edn. Springer, Berlin

Johnson CA, Kelley KD, Leach DL (2004) Sulfur and oxygen isotopes in barite deposits of the western Brooks Range, Alaska, and implications for the origin of the Red Dog massive sulfide deposits. Econ Geol 99:1435–1448

Johnson CA, Emsbo P, Poole FG, Rye RO (2009) Sulfur- and oxygen-isotopes in sediment-hosted stratiform barite deposits. Geochim Cosmochim Acta 73:133–147

Kharaka YK, Hanor JS (2003) Deep fluids in the continents: I. Sedimentary basins. Treatise Geochem 5:605

Kyser TK (2007) Fluids, basin analysis, and mineral deposits. Geofluids 7:238–257

Lawler JP, Crawford ML (1983) Stretching of fluid inclusions resulting from a low-temperature microthermometric technique. Econ Geol 78:527–529

McDonough WF, Sun SS (1995) The composition of the earth. Chem Geol 120:223–253

McRae ME (2017) Barite-2015 [advance release]. U.S. geological survey minerals yearbook-2015

Mohajjel M, Fergusson CL, Sahandi MR (2003) Cretaceous-Tertiary convergence and continental collision, Sanandaj-Sirjan zone, Western Iran. J Asian Earth Sci 21:397–412

Pattan JN, Pearce NJG, Mislankar PG (2005) Constraints in using Cerium-anomaly of bulk sediments as an indicator of paleo bottom water redox environment: a case study from the Central Indian Ocean Basin. Chem Geol 221:260–278

Paytan A, Kastner M, Campbell D, Thiemens MH (1998) Sulfur isotopic composition of Cenozoic seawater sulfate. Science 282:1459–1462

Paytan A, Mearon S, Cobb K, Kastner M (2002) Origin of marine barite deposits: Sr and S isotope characterization. Geology 30:747–750

Radfar J, Kohansal R (undated) Farmahin quadrangle map 1:100000. Geological Survey of Iran

Rajabzadeh MA (2007) A fluid inclusion study of a large MVT barite–fluorite deposit: Komshecheh, Central Iran. Iran J Sci Technol 31:73–87

Roedder E (1984) Fluid inclusions. Reviews in mineralogy, vol 12. De Gruyter, Berlin

Saintilan NJ, Spangenberg JE, Chiaradia M, Chelle-Michou C, Stephens MB, Fontboté L (2019) Petroleum as source and carrier of metals in epigenetic sediment-hosted mineralization. Sci Rep 9:8283

Shepherd TJ, Ranbin AH, Alderton DHM (1985) A practical guide to fluid inclusion studies. Blackie, Glasgow, p 239

Shields G, Kimura H, Yang J, Gammon P (2004) Sulphur isotopic evolution of Neoproterozoic-Cambrian seawater: new francolite-bound sulphate $\delta^{34}S$ data and a critical appraisal of the existing record. Chem Geol 204:163–182

Steele-MacInnis M, Bodnar RJ, Naden J (2011) Numerical model to determine the composition of H_2O–NaCl–$CaCl_2$ fluid inclusions based on microthermometric and microanalytical data. Geochim Cosmochim Acta 75:21–40

Stevens EWN, Bailey JV, Flood BE, Jones DS, Gilhooly WP, Joye SB, Teske A, Mason OU (2015) Barite encrustation of benthic sulfur-oxidizing bacteria at a marine cold seep. Geobiology 13:588–603

Taylor HP (1968) The oxygen isotope geochemistry of igneous rocks. Contrib Miner Petrol 19:1–71

Turchyn AV, Schrag DP (2006) Cenozoic evolution of the sulfur cycle: insight from oxygen isotopes in marine sulfate. Earth Planet Sci Lett 241:763–779

Verdel C, Wernicke BP, Hassanzadeh J, Guest B (2011) A Paleogene extensional arc flare-up in Iran. Tectonics 30:TC3008

Wu Q, Jiang X, Lu Q, Li J, Chen J (2021) Changes in soil organic carbon and aggregate stability following a chronosequence of Liriodendron chinense plantations. J For Res 32:355–362

Zarasvandi A, Zaheri N, Pourkaseb H, Chrachi A, Bagheri H (2014) Geochemistry and fluid-inclusion microthermometry of the Farsesh barite deposit, Iran. Geologos 20:201–214